Inorg. Chem. **2003**, *42*, 1564–1575

Chiral Direction and Interconnection of Helical Three-Connected Networks in Metal-Organic Frameworks

T. J. Prior and M. J. Rosseinsky*

Department of Chemistry, The University of Liverpool, Liverpool L69 7ZD, U.K.

Received June 6, 2002

The control of the interpenetration and chirality of a family of metal-organic frameworks is discussed. These systems contain two- (**A**) and four-fold (**B**) interpenetration of helical three-connected networks generated by binding the 1,3,5-benzenetricarboxylate (btc) ligand to a metal center. These frameworks have the general formula $Ni_3(btc)_2X_mY_n$• solvent (where X = pyridine or 4-picoline, Y = ethylene glycol, 1,2-propanediol, 1,4-butanediol, *meso*-2,3-butanediol, 1,2,6-hexanetriol, glycerol). The structural and chemical effects of modifying the alcohol and aromatic amine ligands bound to the metal center include controlling the thermal stability and the degree of interpenetration. Covalent linking of the four interpenetrating networks in the **A** family and the switching of diol binding from mono- to bidentate are demonstrated. Recognition of chiral diols by the hand of the network helices is investigated by binding an alcohol ligand with two chiral centers of opposite sense to the same helix. This reveals the subtle nature of the helix–ligand interaction.

Introduction

The predictable synthesis of chiral porous solids is a major driving force in the search for new synthetic routes to open-framework materials. Chiral porous solids are attractive synthetic targets on account of their possible applications as molecular sieves and heterogeneous catalysts. The development of enantiopure phases has been attempted by a number of routes, including chiral functionalization of zeolites, chiral templating of metal phosphates and related phases, construction of extended organic solids through hydrogen bonding interactions, and formation of metal-organic coordination polymer frameworks. The predictable synthesis of bulk chiral solids may be accomplished in two ways: (i) growth of enantiopure hosts around a resolved template and (ii) construction of a framework from homochiral building blocks. There are also a significant number of chiral extended solids that crystallize as equal mixtures of two enantiomorphs. Chirality in these materials is derived from the presence of helices within noncentric space groups rather than through a chirally enriched component in the reaction mixture.

Cross-linked protein crystals displaying high porosity have been shown to be capable of separating molecules on grounds of size, structure, and chirality.[1] Chiral hydrogen bonded architectures[2] with sizable cavities (ca. 1400 Å^3) and chiral templating to form homochiral assemblies[3,4] in solution have been demonstrated.

Bulk chiral aluminosilicate zeolites are unknown: zeolite β,[5] like the titanosilicate ETS-10,[6] is multiphasic and retains its enantiopurity over a few crystallographic layers. Gallophosphates[7−9] and aluminophosphates[10] have been grown enantiomerically pure around resolved templates; however, these phases collapse irreversibly upon calcination. A number of chiral open framework phosphates[11−14] and germanates[15] grown from achiral components have been obtained by single crystal growth.

* To whom correspondence should be addressed. E-mail: m.j.rosseinsky@liv.ac.uk.

(1) Vilenchik, L. V.; Griffith, J. P.; St. Clair, N.; Navia, M. A.; Margolin, A. L. *J. Am. Chem. Soc.* **1998**, *120*, 4290−4294.
(2) MacGillivray, L. R.; Atwood, J. L. *Nature* **1997**, *389*, 469−472.
(3) Prins, L. J.; Huskens, J.; De Jong, F.; Timmerman, P.; Rheinhoudt, D. N. *Nature* **1999**, *398*, 498−502.
(4) Prins, L. J.; De Jong, F.; Timmerman, P.; Reinhoudt, D. N. *Nature* **2000**, *408*, 181−184.
(5) Newsam, J. M.; Treacy, M. M. J.; Koetsier, W. T.; de Gruyter, C. B. *Proc. R. Soc. London, Ser. A* **1988**, *420*, 375.
(6) Anderson, M. W.; Terasaki, O.; Ohsuna, T.; Philippou, A.; MacKay, S. P.; Ferreira, A.; Rocha, J.; Lidin, S. *Nature* **1994**, *367*, 347−351.
(7) Lin, C. H.; Wang, S. L. *Inorg. Chem.* **2001**, *40*, 2918−2921.
(8) Lii, K. H.; Chen, C. Y. *Inorg. Chem.* **2000**, *39*, 3374−3378.
(9) Stalder, S. M.; Wilkinson, A. P. *Chem. Mater.* **1997**, *9*, 2168−2173.
(10) Gray, M. J.; Jasper, J. D.; Wilkinson, A. P.; Hanson, J. C. *Chem. Mater.* **1997**, *9*, 976.
(11) Yilmaz, A.; Bu, X. H.; Kizilyalli, M.; Stucky, G. D. *Chem. Mater* **2000**, *12*, 3243.
(12) Simon, N.; Loiseau, T.; Ferey, G. *Solid State Sci.* **2000**, *2*, 389−395.
(13) Bontchev, R. P.; Iliev, M. N.; Dezaneti, L. M.; Jacobson, A. J. *Solid State Sci.* **2001**, *3*, 133−142.

10.1021/ic025775i CCC: $25.00
Published on Web 02/07/2003

Postsynthetic modification of achiral zeolite pores with homochiral metal complexes[16−18] or other chiral modifiers[19] has been demonstrated, and the catalytic possibilities of this approach have been explored.[20,21] One notable example is the dehydration of 2-butanol using zeolite H−Y modified with a chiral dithiane oxide,[22−24] where the rate of conversion for one enantiomer of the alcohol is enhanced relative to the other.

The recent extensive interest in metal-organic frameworks results from the opportunity they offer to control the structure of microporous materials, and significant attention is now being paid to the development of this route to chiral systems. Coordination polymer chemistry has produced a number of molecular frameworks in which chirality is due to the use of resolved building blocks,[25,26] including D-POST-1[27] derived from $[Zn_3(\mu_3\text{-}O)(O_2CR)_6L_3]$ units (O_2CR is a modified D-tartaric acid derivative with a pendant pyridine group). This may be dehydrated to form a crystalline porous solid which displays enantioselective uptake of $Ru(bipy)_3^{2+}$ complexes and may be used to perform enantioselective catalysis.

There are several examples of helical chiral coordination polymers.[28−30] The materials $Zn_2(btc)(NO_3)\cdot H_2O\cdot 5H_2O$[31] (btc = 1,3,5-benzenetricarboxylate) and $Ag(hat)ClO_4\cdot 3CH_3NO_2$ (hat = 1,4,5,8,9,12-hexaazatriphenylene)[28] fall into this category. They are of particular significance for this paper as they contain helical three-connected networks. In principle, the chiral direction of such helical structures may be accomplished by templating via chiral molecules bound to the helix. This is a feasible strategy in coordination polymer chemistry, and one that is explored in detail here. It is the chiral direction of such networks and control of their interpenetration which are the focus of this paper.

(14) Boy, I.; Stowasser, F.; Schafer, G.; Kniep, R. *Chem.—Eur. J.* **2001**, *7*, 834−839.
(15) Gier, T. E.; Bu, X.; Feng, P.; Stucky, G. D. *Nature* **1998**, *395*, 154−157.
(16) Ernst, S.; Fuchs, E.; Yang, X. *Microporous Mesoporous Mater.* **2000**, *35*−*6*, 137−142.
(17) Sabater, M. J.; Corma, A.; Domenech, A.; Fornes, V.; Garcia, H. *Chem. Commun.* **1997**, 1285−1286.
(18) Ogunwumi, S. B.; Bein, T. *Chem. Commun.* **1997**, 901−902.
(19) Page, P. C. B.; Hutchings, G. J.; Bethell, D. *Chim. Oggi* **2001**, *19*, 14−17.
(20) Davis, M. E. *Microporous Mesoporous Mater.* **1998**, *21*, 173−182.
(21) Hutchings, G. J. *Chem. Commun.* **1999**, 301−306.
(22) Feast, S.; Bethell, D.; Page, P. C. B.; King, F.; Rochester, C. H.; Siddiqui, M. R. H.; Willock, D. J.; Hutchings, G. J. *J. Chem. Soc., Chem. Commun.* **1995**, 2409−2411.
(23) Feast, S.; Siddiqui, M. R. H.; Wells, R. P. K.; Willock, D. J.; King, F.; Rochester, C. H.; Bethell, D.; Page, P. C. B.; Hutchings, G. J. *J. Catal.* **1997**, *167*, 533−542.
(24) Wells, R. P. K.; Tynjala, P.; Bailie, J. E.; Willock, D. J.; Watson, G. W.; King, F.; Rochester, C. H.; Bethell, D.; Page, P. C. B.; Hutchings, G. J. *Appl. Catal., A* **1999**, *182*, 75−84.
(25) Ranford, J. D.; Vittal, J. J.; Wu, D. *Angew. Chem., Int. Ed.* **1998**, *37*, 1114−1116.
(26) Kiang, Y. H.; Gardner, G. B.; Lee, S.; Xu, Z. T.; Lobkovsky, E. B. *J. Am. Chem. Soc.* **1999**, *121*, 8204−8215.
(27) Seo, J. S.; Whang, D.; Lee, H.; Jun, S. I.; Oh, J.; Jeon, Y. J.; Kim, K. *Nature* **2000**, *404*, 982−986.
(28) Abrahams, B. E.; Jackson, P. A.; Robson, R. *Angew. Chem., Int. Ed.* **1998**, *37*, 2656.
(29) Biradha, K.; Seward, C.; Zaworotko, M. J. *Angew. Chem., Int. Ed* **1999**, *48*, 492−495.
(30) Batten, S. R.; Hoskins, B. F.; Robson, R. *Angew. Chem., Int. Ed. Engl.* **1997**, *36*, 636−637.
(31) Yaghi, O. M.; Davis, C. E.; Li, G. M.; Li, H. L. *J. Am. Chem. Soc.* **1997**, *119*, 2861−2868.

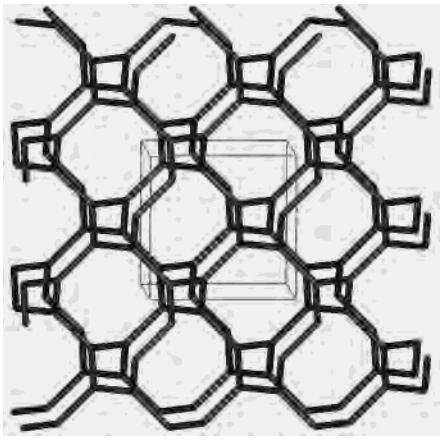

Figure 1. A single (10,3)-a network. The most symmetric cubic form is shown (nodes occupy the 8a positions in space group $I4_132$). Each node is three-connected. The net contains chiral four-fold helices running parallel with the three cubic axes.

We have recently shown[32,33] that neutral M_3btc_2 three-connected nets based on the 1,3,5-benzenetricarboxylate ligand adopt the helical (10,3)-a network (Figure 1).

They afford a broad family of chiral solids featuring two- or four-fold interpenetration of these networks (Figure 2), with void volumes of up to 50%, accessible upon careful removal of the pore solvent. The transition metal cations act as linear connectors between the tridentate btc ligands which adopt *trans* locations in the octahedral coordination sphere of the metal. These two components are the network formers. The octahedral coordination at the metal centers in these materials is completed by *cis* pyridine and alcohol groups, which play a key role in determining the three-dimensional nature of the structure via hydrogen bonding to the btc network former. These auxiliary ligands must play a key role in defining which of the competing two- and four-network structures forms, but although there is considerable structural diversity, no clear chemical design principles for controlling this have emerged. Monodentate ethylene glycol (**A**) and bidentate 1,2-propanediol (**B**) are the ligands directing the formation of the parent examples of the four network and two network phases, respectively. Modification of the metal-binding characteristics of the auxiliary ligands further offers the ability to control the thermal stability of the networks. The presence of these auxiliary ligands offers a mechanism for controlling the helix chirality: the configuration at a chiral alcohol or pyridine in principle can influence the sense of the helices defining the chirality of the solid. This *chiral templating* by the ligand was seen in the case of 1,2-propanediol directing the handedness of the 10,3-a network helices, with left-handed helices occurring with binding of the *S* enantiomer of the diol.[33] The microscopic interactions responsible for the selection of this diasteroisomeric combination of helix hand and enantiomer were identified, but it remains to test the limits of the predictive power of this model when applied to other systems. In particular, no chiral diols were stabilized bound to the metal in the four network

(32) Kepert, C. J.; Rosseinsky, M. J. *Chem. Commun.* **1998**, 31−32.
(33) Kepert, C. J.; Prior, T. J.; Rosseinsky, M. J. *J. Am. Chem. Soc.* **2000**, *122*, 5158−5168.

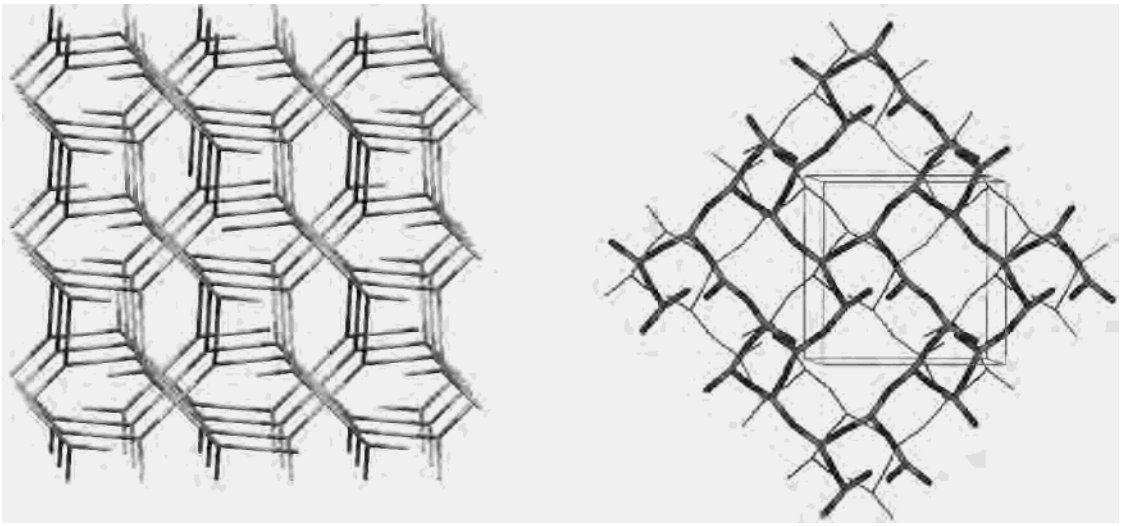

Figure 2. (a) Four-fold **A** and (b) two-fold **B** interpenetration of the (10,3-a) network to form the two framework structures dealt with in this paper.

structure, removing the possibility of chirally templating this thermally more stable phase.

In this paper, we examine the effect of simple chemical modification of the auxiliary alcohol and aromatic amine ligands bound to the metal on network formation, interpenetration, thermal stability, and chirality. The extent to which true templating can be effected in this class of materials is investigated using potential template molecules "carried" in inert solvents. The results reveal an extraordinary ability to tune the details of the structure by such modifications while maintaining the same network types.

Experimental Section

Synthesis. The majority of the crystals used for structure solution were prepared by vapor diffusion of the volatile base (pyridine or 4-methyl pyridine (4-picoline)) into a stoichiometric 3:2 molar ratio solution of $Ni(NO_3)_2 \cdot 6H_2O$ and 1,3,5-benzenetricarboxylic acid dissolved in the alcohol (ethylene glycol, 1,2-propanediol, 1,4-butanediol, or 1,2,6-hexanetriol). A 2 mL portion of an alcoholic solution of the solid reagents was placed in a cylindrical specimen jar, height 75 mm, diameter 25 mm. Approximately 2.5 mmol (45-fold molar excess over $Ni(NO_3)_2 \cdot 6H_2O$) of the volatile base was placed in a stoppered vial. The vial was placed within the jar and its stopper pierced. The jar was then sealed and left to stand. The concentration of the reagents within the solvent was typically on the order of 1×10^{-2} mol dm^{-3} in H_3btc. These procedures readily afford polycrystalline product using 1,4-butanediol so that in this case the procedure was adapted as follows by extremely slow vapor diffusion of pyridine over a period of approximately 18 months. A solution (1 mL) of 3:2 stoichiometric $Ni(NO_3)_2 \cdot 6H_2O$ and H_3btc (5.95 mM in H_3btc) was placed in a sample jar (height 50 mm, diameter 15 mm) which was stoppered and the stopper pierced with a single pin prick. A similar procedure was carried out with 0.2 mL of pyridine. Both sample jars were loaded into a solids bottle of volume 320 cm^3 which was sealed and left undisturbed at room temperature.

In the case of the glycerol/pyridine phase, 5 mL of an alcoholic solution of metal nitrate (0.036 molar) and 1,3,5-benzenetricarboxylic acid (0.024 molar) was placed in a test tube. Pure solvent (15 mL) was carefully layered on top of this solution. Base (6.3 mmol, 45-fold excess, 0.5 mL) was layered on top of the pure solvent. The test tube was sealed and allowed to stand undisturbed at room temperature.

The use of *meso*-2,3-butanediol is complicated slightly by its melting point being 32 °C. Standard vapor diffusion methods were employed, but the reaction was carried out at a constant temperature of 33 °C. Good sized single crystals were obtained after pyridine vapor had been allowed to diffuse into a glycolic mixture of $Ni(NO_3)_2 \cdot 6H_2O$ and H_3btc for approximately 2 weeks.

The solid *R*-1,2-phenylethanediol may be used as a ligand to the divalent nickel cation when it is dissolved in a nonbinding solvent and standard vapor diffusion procedures are applied. $Ni(NO_3)_2 \cdot 6H_2O$ (0.05 g, 0.1722 mmol), H_3btc (0.025 g, 0.1190 mmol), and *R*-1,2-phenylethanediol (0.10 g, 0.725 mmol) were dissolved in 10 mL of benzyl alcohol with stirring. This solution was divided in 5 portions, and using standard vapor diffusion techniques, pyridine vapor was introduced into them. This afforded green-blue octahedral crystals after a period of approximately 2 weeks.

Crystallography. Data were recorded on a Stöe IPDS instrument at 193 K using graphite monochromated Mo Kα radiation. Data were reduced using Stöe IPDS software. In the case of the 1,2-propanediol/4-picoline, *meso*-2,3-butanediol, glycerol, and 1,2,6-hexanetriol phases, the crystals were too small or weakly diffracting to permit structure solution using the laboratory instrument, and data were collected on station 9.8 of the Daresbury Laboratory Synchrotron Radiation Source using a Bruker AXS SMART CCD area detector diffractometer, with the crystals cooled to 150 K using an Oxford Cryosystems nitrogen cryostream. Data were integrated using Bruker software[34] and corrected semiempirically[35] for beam decay and absorption. Structures were solved by a combination of direct methods and Fourier syntheses within SHELX-97[36,37] and refined using full-matrix-least squares refinement. Important crystallographic details are given in Table 1.

Thermal Analysis. TGA data were collected on a Seiko Instruments EXSTAR TG/DTA 6030 under flowing helium at 300 mL min^{-1} at a heating rate of 2 °C min^{-1}.

(34) *SMART (control) and SAINT (integration) software*, 4th ed.; Bruker AXS Inc.: Madison, WI, 1994.
(35) Sheldrick, G. M. *SADABS*; Universität Gottingen: Gottingen, Germany, 1997.
(36) Sheldrick, G. M. *SHELXS-97*; Universität Gottingen: Gottingen, Germany, 1997.
(37) Sheldrick, G. M. *SHELXL-97: Program for the refinement of crystal structures*; Universität Gottingen: Gottingen, Germany, 1997.

Table 1. Chemical Composition and Crystallographic Details of the Interpenetrating (10,3)-a Network Phases Studied in This Paper

	A	**B**	**1**	**2**	**3**	**4**	**5**	**6**	**7**
chemical formulation	$Ni_3(btc)_2(py)_6(eg)_6$·3(eg)·4(H_2O)	$Ni_3(btc)_2(py)_6(1,2\text{-pd})_3$·11(1,2-pd)·8($H_2O$)	$Ni_3(btc)_2(py)_6(1,4\text{-bd})_4$·($\mu$-1,4-bd)·2(1,4-bd)	$Ni_3(btc)_2(4\text{-pic})_6$·(eg)$_6$·guest	$Ni_3(btc)_2(4\text{-picoline})_6$·(1,2-pd)$_6$·guest	$Ni_3(btc)_2(py)_6$(*meso*-2,3-butanediol)$_3$·guest	$Ni_3(btc)_2(py)_6$(*R*-Phenylethyleneglycol)$_3$·guest	$Ni_3(btc)_2(py)_6$-(1,2,6-hexanetriol)$_3$·guest	$Ni_3(btc)_2(py)_6$-(glycerol)$_x$·guest $x \approx 4.3$
$Ni_3(btc)_2X_mY_n$·guest	X = py Y = ethylene glycol	X = py Y = 1,2-propanediol	X = pyridine Y = 1,4-butanediol	X = 4-picoline Y = ethylene glycol	X = 4-picoline Y = 1,2-propanediol	X = pyridine Y = *meso*-2,3-butanediol	X = pyridine Y = (*R*)-phenyl ethylene glycol	X = pyridine Y = 1,2,6-hexanetriol	X = pyridine Y = glycerol
fw	see refs 32 and 33		1551.33	1523.39	1571.45	1497.45	1286.97	1521.36	1520.19
a/Å			16.312(1)	31.946(3)	32.226(1)	28.400(4)	28.718(2)	28.8037(18)	28.6020(15)
c/Å			30.060(3)						
V/Å^3			7998(1)	32603(5)	33468(2)	22906(5)	23685(3)	23897(3)	23399(2)
space group (No.)			$P4_322$ (95)	$F4_132$ (210)	$F4_132$ (210)	$I4_132$ (214)	$I4_132$ (214)	$I4_132$ (214)	$I4_132$ (214)
T/°C			−80(2)	−80(2)	−123(2)	−123(2)	−80(2)	−123(2)	−123(2)
λ/Å			0.71073	0.71073	0.68920	0.69410	0.71073	0.68920	0.69230
Z			4	16	16	8	8	8	8
ρ_{calcd}/Mg m^{-3}			1.288	1.241	1.247	0.858	0.722	0.845	0.863
μ_{calcd}/mm^{-1}			0.721	0.708	0.690	0.503	0.480	0.482	0.495
final R indices[a]			R = 0.0641	R = 0.0842	R = 0.0563	R =0.0669	R = 0.0998	R = 0.0629	R = 0.0834
[$I > 2\sigma_I$]			R_w = 0.1440	R_w = 0.2088	R_w = 0.1711	R_w = 0.2097	R_w = 0.2840	R_w = 0.1906	R_w = 0.2289
void V/%	28	51	14.3	16.4	14.3	50.7		60.6	35.8
hand of helices	right	right	left	left	left	left	right	left	left
enantiomer bound to helices	achiral	*R*	achiral	achiral	60(1)% *S* 40(1)% *R*	achiral	*R*	*S*	achiral

[a] Quality factors defined as $R = \sum||F_o| - |F_c||/\sum|F_o|$, $R_w = \sqrt{\sum(w(F_o^2 - F_c^2)^2)/\sum(wF_o^4)}$.

Chiral GC Analysis. Single crystals were digested in the minimum volume of acetic acid and ethyl acetate. GC data were collected using a Shimadzu GC-148 chromatogram with a Supelco α-cyclodextrin column operating at 70 °C. Data were collected from two single crystals, each being recorded four times.

Results

The phases prepared from systematic variation of the nature of the auxiliary ligands bound to the octahedral metal center are most usefully discussed by division into the two- and four-network phases.

Four Network Phases. These are discussed with reference to the structure and properties of the parent four-network phase[33] with ethylene glycol and pyridine auxiliary ligands coordinated to the octahedral metal center, referred to as **A** in the subsequent text and in Table 1.

1,4-Butanediol as an Auxiliary Ligand. Although the 1,4-butanediol (1,4-bd) derived framework **1** consists of four interpenetrating 10,3-a networks, it crystallizes in a tetragonal space group rather than the cubic structure of the parent ethylene glycol phase.[33] Structure **1** adopts the enantiomorphous pair of space groups $P4_122$ (No. 91) and $P4_322$ (No. 95). For the crystal examined, the model employed uses $P4_3$-22, and the refined Flack parameter of zero indicates this is the correct choice of enantiomorph, with interpenetration of four networks of the same handedness. The asymmetric unit contains two independent nickel cations in approximately octahedral coordination (Figure 3a). The crystallographic formulation of **1** is $Ni_3(btc)_2(py)_6(1,4\text{-bd})_4(\mu\text{-}1,4\text{-bd})\cdot 2(1,4\text{-bd})$. There is one guest molecule located in the asymmetric unit, with poorly resolved alkyl chains, referred to in the formula in parentheses following the center dot. Two *trans* btc carboxylates are linked by the nickel cation, and the coordination of nickel is completed by two *cis* pyridine and two *cis* alcohol ligands. Each alcohol forms a hydrogen bond to the carbonyl oxygen of btc, ensuring that the carboxylates are approximately orthogonal in orientation.

However, there is a very significant difference between the coordination at the two nickel cations which is the cause of the tetragonal distortion. At Ni1, both of the 1,4-butanediol ligands are monodentate, as for the previously described four-network interpenetrating phases. At Ni2, one of the 1,4-butanediol ligands bridges to another symmetry equivalent Ni2 cation in a neighboring (10,3-a) network as depicted in Figure 3b. The effect of this is that $^1/_5$ of the 1,4-butanediol ligands link different networks, forming the first example of (10,3)-a networks cross-linked by covalent coordinative bonding (Figures 3c and 4). In total, there are four molecules of 1,4-butanediol cross-linking networks in each unit cell, resulting in all the networks being cross-linked with $^2/_3$ of the nickel nodes involved in cross-linking. Network interpenetration is commonly observed in coordination polymer chemistry, but this appears to be the first example of covalent linking of such networks.

The view down the crystallographic *c* axis (Figure 4c) shows cross-linking is confined to the helices within the networks in this direction, while for the *a* and *b* directions cross-linking occurs outside these helices. In **1**, the four

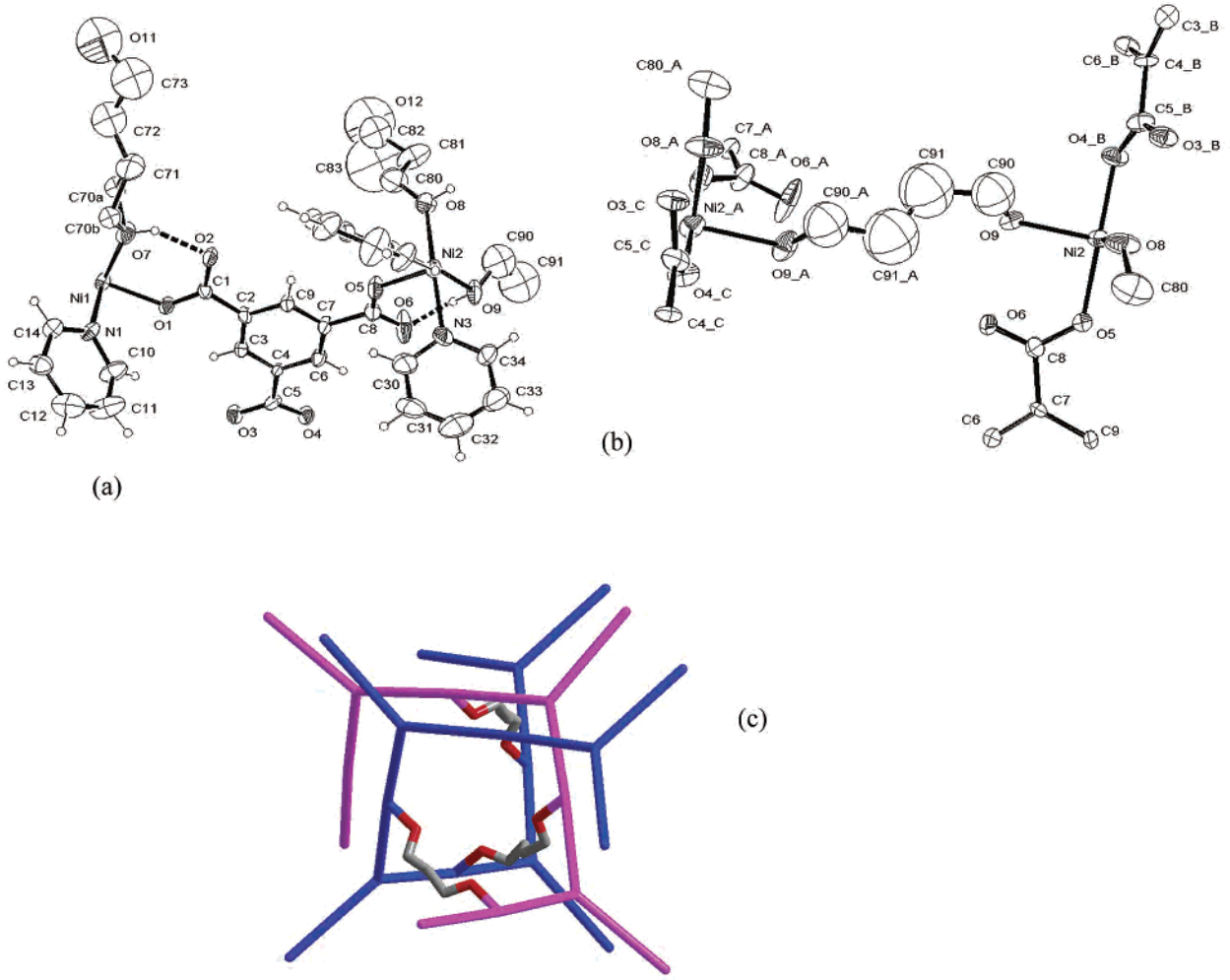

Figure 3. (a) ORTEP plot of the framework atoms in the asymmetric unit of **1**, $Ni_3(btc)_2(py)_6(1,4\text{-bd})_4(\mu\text{-}1,4\text{-bd})\cdot 2(1,4\text{-bd})$. Atoms are shown as 30% thermal ellipsoids. Selected non-hydrogen atoms are labeled. Note the hydrogen bonds O2···O7 and O6···O9. (b) A single 1,4-butanediol molecule linking two nickel cations in adjacent (10,3-a) networks in **1**. Atoms are shown as 30% thermal ellipsoids. Hydrogen atoms, pyridine ligands, and the chains of monodentate 1,4-butanediol ligands have been omitted. Symmetry equivalent atoms are generated using the following symmetry operators: A = $-1+y$, $1+x$, $^1/_4-z$; B = $1-y$, $1+x$, $^1/_4+z$; C = x, $2-y$, $^1/_2-z$. (c) Cross-linking of two (10,3)-a networks by 1,4-butanediol. One network is colored blue, the other magenta. Btc centroids are represented as trigonal nodes, joined by linear Ni^{2+} nodes. 1,4-Butanediol is shown in gray (carbon atoms) and red (oxygen atoms).

networks are therefore linked into two sets of cross-linked pairs related by a unit translation along *a* or *b*. The distance between linked nickel cations in adjacent networks (Ni2 and Ni2_A in Figure 3b) is 9.547(1) Å, while similar distances in the *xy* plane are 9.321(1) and 10.234(1) Å, showing that the bidentate bridging nature of 1,4-butanediol is strongly dependent upon the intercation distance. In the cubic network, the analogous nickel to nickel distance is 9.750(1) Å. The tetragonal distortion from the ethylene glycol phase **A** to **1** is accompanied by an expansion of the *xy* plane by approximately 5% and an increase in the *c* axis to 6% less than double the cubic lattice parameter of the parent because of the linking 1,4-butanediol.

Narrow pores with openings of 2.2 Å (defined as distance between van der Waals surfaces) which run parallel with the unit cell axes persist despite the cross-linking of networks, although the solvent accessible volume[38] is only 14.3% compared with 28% in the non-cross-linked ethylene glycol parent. Four cavities of 245 $Å^3$ (3.1% of unit cell volume) are centered on the 4a positions, defined by closest atom to atom distances of 2.9 Å to C83 and 3.6 Å to O12, which are part of one of the monodentate alcohols bound to the framework.

The enhanced rigidity imparted by the 1,4-butanediol could be expected to manifest itself in greater thermal stability than for phases with no cross-linking. Thermogravimetric data for **1** under flowing helium are shown in Figure 5a. The loss of mass with heating is concentrated into three major changes. The first loss, upon heating to 140 °C, of approximately 15% corresponds to that calculated for the loss of the two crystallographically observed molecules of 1,4-butanediol pore solvent for every Ni_3btc_2 formula unit. Heating to 200 °C results in the loss of a further 35% mass to generate a phase with calculated composition $Ni_3btc_2(py)_2(\mu\text{-}1,4\text{-bd})$, consistent with retention of the bridging but loss of the monodentate butanediol ligands. Heating above 360 °C results in complete collapse of the material and is

(38) Spek, A. L. *Acta Crystallogr., Sect. A* **1990**, *46*, C34.

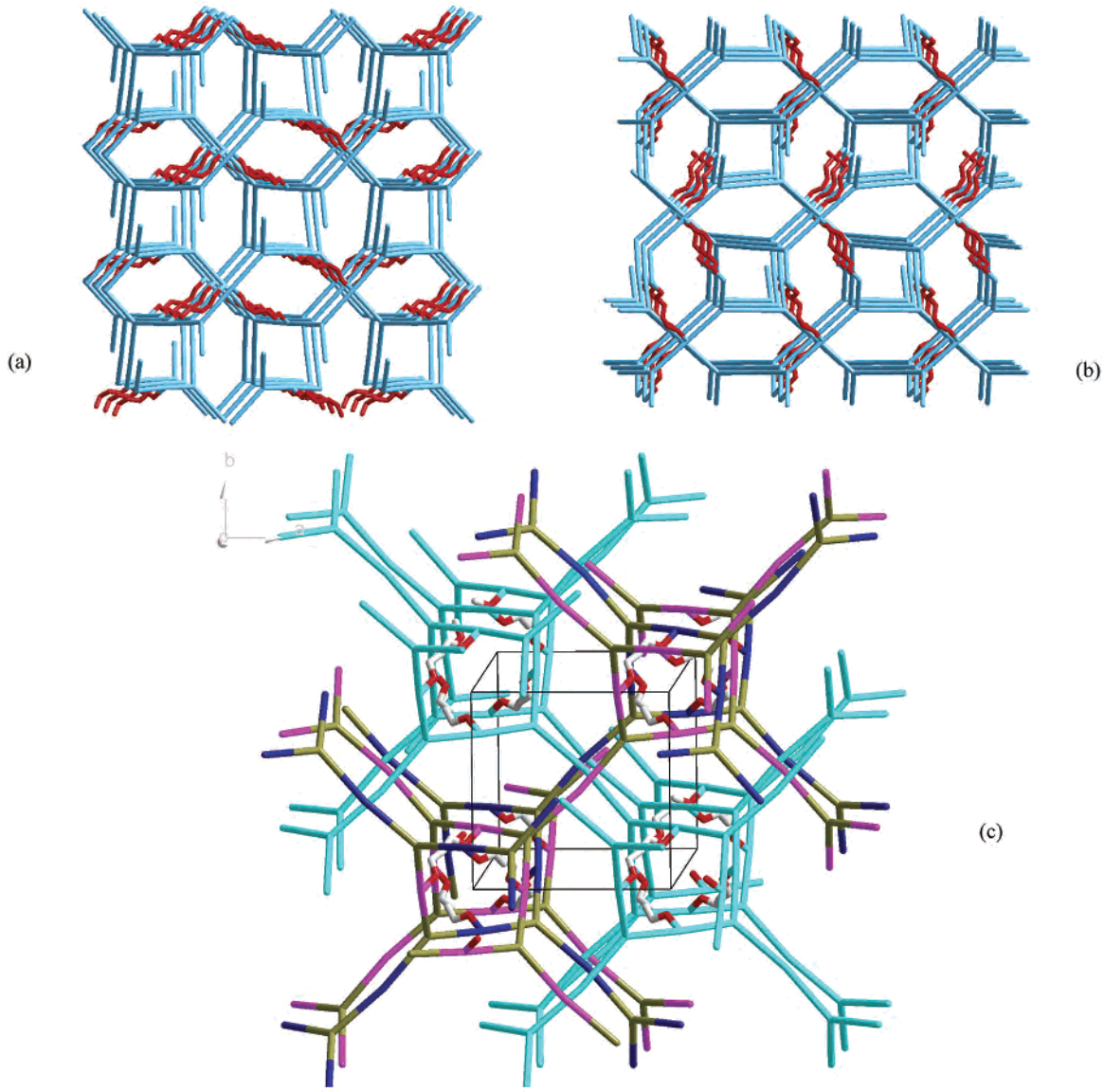

Figure 4. Cross-linking of (10,3)-a networks in **1**, $Ni_3(btc)_2(py)_6(1,4\text{-bd})_4(\mu\text{-}1,4\text{-bd})\cdot 2(1,4\text{-bd})$. Btc centroids are trigonal nodes joined by linear Ni^{2+} nodes, both colored light blue. Cross-linking 1,4-butanediol is colored red. (a) View down *a*. (b) View down *b*. (c) View down *c*. On viewing the unit cell along *c*, there are four sets of helices visible, each of which involves interpenetration of two of the four networks and is internally cross-linked, related by translation across the face diagonal of the cell. One of these pairs is shown with all the nodes in cyan, the other with the btc nodes in brown and the Ni nodes in the two distinct networks in the pair as purple and dark blue, respectively. Part a shows unlinked four-fold interpenetrated nets.

accompanied by a rapid mass change as the organic component burns off. X-ray powder diffraction data collected following heating to 140 °C reveal that **1** remains highly crystalline as illustrated in Figure 5b and Table S1 (Supporting Information) in contrast to the decrease in crystallinity[33] upon guest removal from the parent **A**. The unit cell changes little on desolvation; a small contraction along *c* is observed while the *xy* plane remains largely unchanged and the cell volume decreases by 0.65%. X-ray powder diffraction data collected following heating to 180 °C show the phase to be amorphous following mass loss 2.

No rapid or significant reabsorption of ethanol into the pores occurs at room temperature when the 140 °C desolvated material is exposed to an ethanol stream. The material contains significant extra-framework volume, although this is not accessible to ethanol. This is probably a consequence of the narrow pore windows. It is possible that, at elevated temperatures necessary for desolvation, there is sufficient thermal energy for the windows to distort and allow the efflux of solvent, while at room temperature the necessary distortion cannot occur. There is a limited uptake of water into the material produced by heating to 140 °C. The mass increase labeled 1 in Figure S2 of 4.5% corresponds to the uptake of four molecules of water (calculated mass 4.64%) per Ni_3btc_2 unit to produce a material with composition $Ni_3(btc)_2(py)_6(1,4\text{-bd})_4(\mu\text{-}1,4\text{-bd})(H_2O)_4$. The narrow entrances to the pores prevent uptake of molecules larger than water at ambient temperature. Although the extensive cross-linking reported here reduces both the pore volume and the dimensions of the windows giving access to it, the role of 1,4-butanediol as a unique network linker is established. It may in future be possible by judicious choice of synthetic conditions to use this linkage in a sparse manner to produce thermally robust but less dense networks.

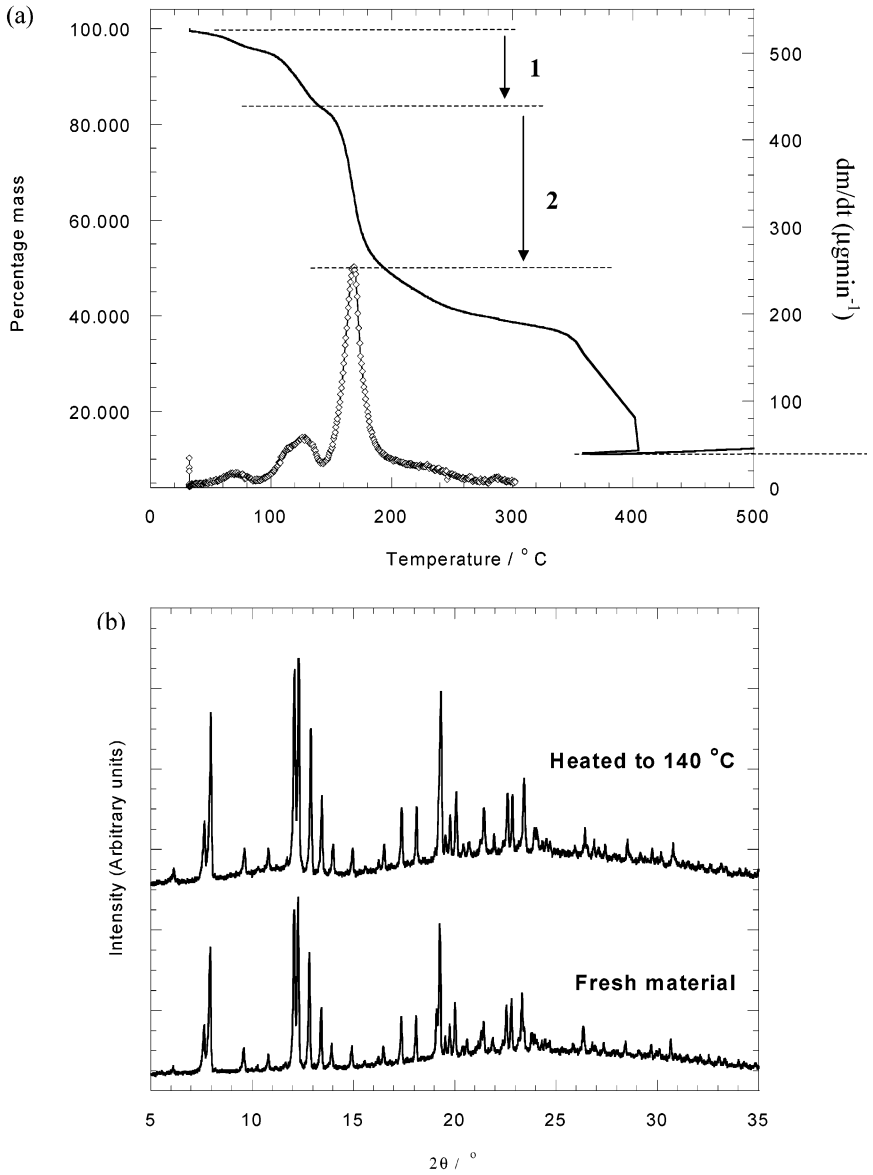

Figure 5. (a) Thermogravimetry for **1**, $Ni_3(btc)_2(py)_6(1,4\text{-bd})_4(\mu\text{-}1,4\text{-bd})\cdot 2(1,4\text{-bd})$. The upper trace is the variation of mass with temperature, while the lower trace is the rate of change of this curve to 300 °C. (b) X-ray powder diffraction patterns for fresh and desolvated **1**, $Ni_3(btc)_2(py)_6(1,4\text{-bd})_4(\mu\text{-}1,4\text{-bd})\cdot 2(1,4\text{-bd})$, show that the material is highly crystalline following heating to 140 °C. The changes in width of selected Bragg reflections are given in Table S1.

4-Picoline as an Auxiliary Ligand. The use of 4-picoline in place of pyridine was an attempt to enhance the thermal stability of the four network phases through the use of the more electron rich methyl pyridine. This material, **2**, has the crystallographic formulation $Ni_3(btc)_2(4\text{-pic})_6(eg)_6\cdot 2H_2O$ and crystallizes in the chiral space group $F4_132$, determined unambiguously from the systematic absences. The structure of this material is chemically almost identical in nature to that of **A**, displaying octahedral coordination of the nickel cations within an enantiopure assembly of four interpenetrating (10,3)-a Ni_3btc_2 networks.

The major difference between pyridine-derived **A** and 4-picoline-derived **2** is the change in cell size and space group. Both phases are cubic, but whereas the **A** crystallizes in $P4_232$ with lattice parameter 15.992(1) Å, **2** crystallizes in $F4_132$ with *a* equal to 31.946(3) Å. The doubling of the cell parameter necessitates a change from a 4_2 screw axis to 4_1 to preserve the pitch of the helix. The composition of the framework in the asymmetric units of the two phases differs only by the addition of a methyl group to pyridine (Figure S3). However, for **A**, the equatorial ligand set displays positional disorder, and the framework benzenetricarboxylate ions occupy two orientations, while the nickel cation is located on the Wyckoff 6f site which has 2.22 site symmetry. It is notable, however, that the 4-methyl substitution on the pyridine auxiliary ligand produces a considerably more locally ordered structure. This may be a consequence of the reduced extra-framework volume compared with the parent phase. Some disorder is present within the ligand set as the ethylene glycol molecules occupy two orientations in the ratio 3:2. However, there is no evidence in the final difference Fourier map for positional disorder of the 4-picoline and ethylene glycol ligands around the metal, which does occur for the pyridine analogue. The larger 4-picoline ligand is

unable to occupy the same position as the diol, driving the ordering of the auxiliary ligands. For **2**, positional disorder in the equatorial ligand set and the framework is not present, which means the local symmetry of the cation is only ..2, and thus, the framework does not crystallize in $P4_232$. Doubling of the unit cell edges and face centering of the resultant cell produces a cell with symmetry $F4_132$. Within $F4_132$, the nickel cation may reside on the Wyckoff 48g position which has ..2 site symmetry, and it then has the correct position with respect to the helix to produce four helical networks. Similar reasoning applies to the aromatic ring of the btc: in the pyridine parent phase, it is centered on the .32 Wyckoff 4b position and disordered over two positions about the two-fold axis, while in **2** it occupies the Wyckoff 32e position which has site symmetry .3. and is not disordered.

The addition of a methyl group to the framework accompanying the change from pyridine to 4-picoline reduces the extra-framework volume to 16.4%. Within the unit cell, cavities with volumes 280 and 230 Å^3 are located on 8a and 8b positions, respectively. These are accessible through openings defined by parallel aromatic rings of 4-picoline ligands whose van der Waals surfaces are 2.4 Å apart.

The mass loss upon heating **2** (Figure S4) does not occur in well-defined steps. There is a small mass loss upon heating to 120 °C of approximately 4% which corresponds to loss of three and a half molecules of water for each Ni_3btc_2 unit (calcd 4.1%). Further heating results in loss of equatorial ligands and eventually a composition close to Ni_3btc_2, shortly before collapse around 360 °C. The calculated composition at 200 °C is $Ni_3btc_2(4\text{-pic})_4$.

4-Picoline produces a more ordered four network structure than pyridine when ethylene glycol is the second auxiliary ligand. Although this cannot be interpreted as stabilization of the four network structure (the thermal stability of the phase is not enhanced), the structure of the 1,2-propanediol 4-picoline phase **3** does point to the 4-picoline strongly favoring the four network structure.

Analysis of single crystal diffraction data suggests a composition $Ni_3(btc)_2(4\text{-picoline})_6(1,2\text{-pd})_6\cdot 2(1,2\text{-pd})$ for **3**. The space group is $F4_132$. The crystal structure is almost identical to that of **2** apart from the introduction of *monodentate* 1,2-propanediol in place of ethylene glycol, reducing the extra-framework volume to 14.3%. This small difference is surprising as previous 10,3-a network phases containing 1,2-propanediol involve bidentate binding to the metal, producing the two-fold interpenetrated structure. It is significant because, for the first time in the four-network case, bound to each chiral network is a chiral ligand. The 1,2-propanediol is monodentate to the metal cation through its primary alcohol function, while the more hindered secondary end of the molecule forms a hydrogen bond to another network (Figure 6a). Thus, the oxygen positions of both the primary and secondary alcohol functions are well-defined. The carbon atoms of the glycol were somewhat poorly resolved for the laboratory X-ray data, in particular at the chiral center, but the synchrotron data allow a full resolution of the enantiomer distribution. Refinement against the

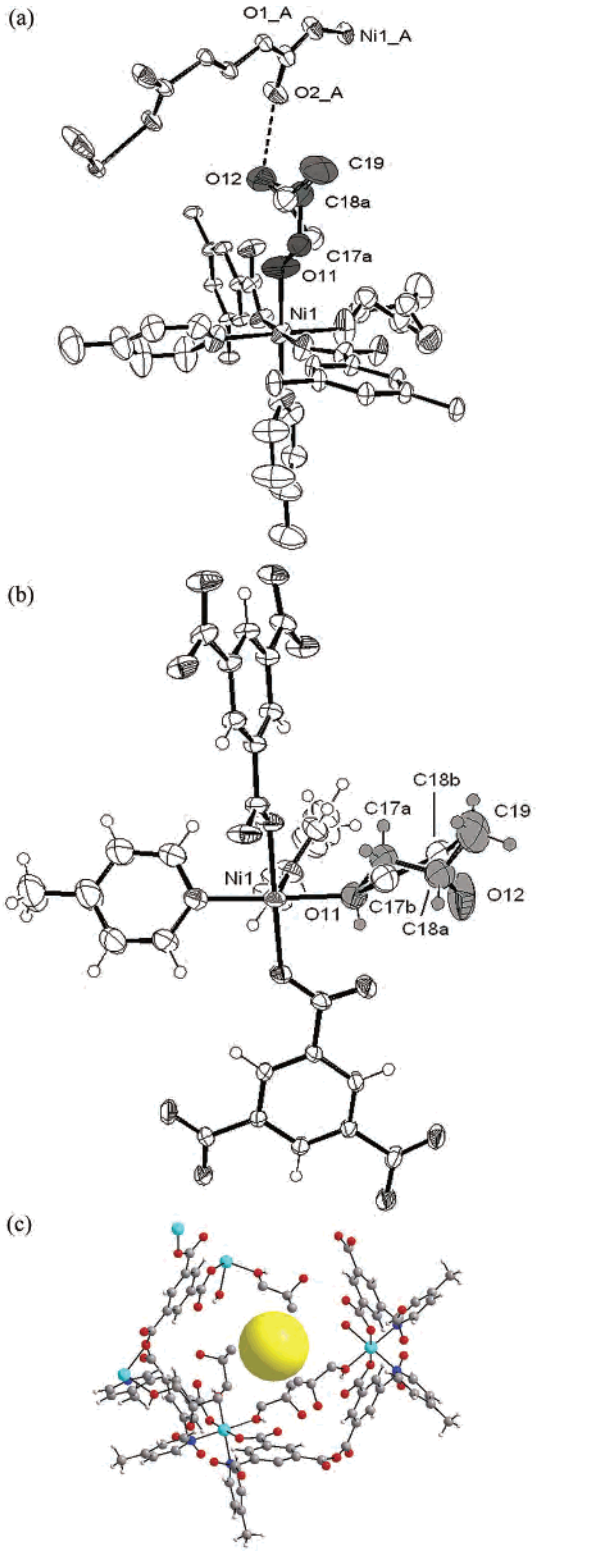

Figure 6. (a) Monodentate 1,2-propanediol forms a hydrogen bond to an adjacent network in **3**. The *S* enantiomer which is 60% occupied is colored gray. The hydrogen bond between O2_A and O12 (2.713(5) Å) is shown as a dashed line. Atoms are shown as 50% thermal ellipsoids. Symmetry equivalent atoms are given by the symmetry operator A = $-^1/_4 - z$, $^1/_4 - y$, $-^1/_4 - x$. (b) One of the two monodentate 1,2-propanediol diol molecules bound at the nickel cation. The major enantiomer is shaded gray. For clarity, the second monodentate orientation produced by a two-fold rotation axis is not illustrated. (c) The methyl groups of the 1,2-propanediol in **3** project toward a pocket of extra-framework space centered on the Wyckoff 16c position which is highlighted as a yellow sphere. Only the major enantiomer is drawn.

synchrotron data using a model in which both enantiomers of 1,2-propanediol are bound to the metal gives a 60/40(1) *S*/*R* distribution of enantiomers in the crystal studied. Two monodentate diols are bound at each metal center, which are related by a two-fold rotation. At each coordination site, a mix of both *S* and *R* enantiomers is present. Figure 6b shows the major enantiomer highlighted in gray at one of the coordination sites.

Within the crystal examined, the four (10,3)-a networks all possess left-handed helices. The 20% enantiomeric excess of the *S*-1,2-propanediol suggests that the helical network is capable of some recognition of the *S* enantiomer, but to a limited extent, in contrast with the two-fold interpenetrated structures where only one enantiomer is bound to a given helix.[33] It is important to note, though, that the left-hand helix *S* enantiomer recognition is the same as that established in the two network phases. The two positions of C18, that is, C18a and C18b in the *S* and *R* enantiomers, respectively, have different closest contacts to the framework. C18a lies 3.628(8) Å from one of the hydrogen atoms on the 4-picoline in the neighboring network. The analogous atom to atom distance for C18b is 3.18(1) Å. It is perhaps unexpected to find the methyl group of the propanediol in a single position; its refined position places it pointing toward a small pocket of extra-framework space of approximately 72 Å^3 centered on the Wyckoff 16c position at $^1/_8$, $^5/_8$, $^5/_8$ (Figure 6c). The energy difference between binding of the two enantiomers may be sufficient that only the left-handed network is obtained when crystals are grown from resolved *S*-1,2-propanediol. This remains speculation currently, and it is notable that this templating is unlikely to be as definitive as in other similar systems where only a single enantiomer is bound to a network of a given hand.

Chiral gas chromatography performed for single crystal samples of **3** suggests that the 1,2-propanediol within single crystals is not racemic with a 47.0(3)/53.0(3) *S*/*R* ratio observed. Considering a composition $Ni_3(btc)_2(4\text{-picoline})_6(1,2\text{-pd})_6\cdot 2(1,2\text{-pd})$, where 60% of the 1,2-propanediol bound to the metal is, say, the *R* enantiomer, while the other solvent is racemic, the expected ratio of enantiomers would be 42.5/57.5 *S*/*R*, which is of the correct magnitude to fit the observed data.

Thermogravimetric analysis data for **3** are shown in Figure S5. There are three major weight losses. Upon heating to 80 °C, a sharp mass loss of 7% is observed which corresponds to the loss of encapsulated guest 1,2-propanediol (calculated mass loss 9.6%). Degradation of the framework begins at 130 °C and corresponds to ligand loss to leave a phase with calculated composition $Ni_3btc_2(4\text{-pic})_{3.8}$ at 180 °C. Further heating above this temperature results in final degradation of the framework and complete collapse above 345 °C. X-ray diffraction data collected following heating to 180 °C show that by this temperature the phase has become amorphous.

Two Network Phases. These systems are discussed with respect to the parent phase **B** with pyridine and 1,2-propanediol auxiliary ligands bound to the metal center.

***meso*-2,3-Butanediol.** The two-network phases are of particular interest because of the recognition of bound alcohol enantiomers by the chiral helices. For a network of particular handedness, one enantiomer of 1,2-propanediol is bound favorably at the metal: the methyl group of the disfavored enantiomer would be found in an energetically unfavorable site close to the framework. The *meso* form of 2,3-butanediol is achiral, but its use as a ligand is interesting because it gives an insight into the templating effect of the diols with alkyl groups bound to the framework. For *meso*-2,3-butanediol, there are two methyl groups present and two stereogenic centers of opposite handedness. Were the *meso*-2,3-butanediol to bind in bidentate fashion at the metal center, one methyl group would point away from the framework ("favored"), while the other would necessarily point toward the homochiral network ("disfavored"). The structure obtained from the use of pure *meso*-2,3-butanediol with pyridine as an auxiliary ligand in **4** is instructive as it is entirely analogous to that for 1,2-propanediol, that is, two interpenetrating (10,3)-a networks of the same hand which are related by the body-centering translation. The Flack parameter for the final refinement is zero within error suggesting the model used is the correct enantiomorph. The *meso*-2,3-butanediol is indeed observed binding in bidentate fashion to the metal. It is disordered equally over two sites related by a two-fold rotation.

The asymmetric units differ only in the change of 1,2-propanediol for *meso*-2,3-butanediol. The coordination of the nickel cation in both phases is shown in Figure 7. In both cases, the diol ligand is disordered over the two-fold axis in two 50% occupied orientations (it is important to note that the orientations are related by a two-fold axis, so this does not correspond to binding both enantiomers). The *S*-enantiomer of 1,2-propanediol in **B** is bound with C11 fully occupied and C12 half occupied. For *meso*-2,3-butanediol in **4**, both the (*S*,*R*) and the (*R*,*S*) isomers are bound with C11 fully occupied and C12a and C12b half occupied. The coordination environments of the nickel cation in the two structures are slightly different as some small distortions are observed when the 2,3-butanediol binds to the cation. Selected bond lengths and angles for the two crystal structures are given in Table 2 to allow comparison of binding the disfavored chiral center of *meso*-2,3-butanediol with the disfavored enantiomer of 1,2-propanediol.

The cubic unit cells at 150 K for the two phases differ very slightly and, as a consequence of that, similar bond lengths for the 2,3-butanediol framework **4** would be expected to be approximately 1% shorter than those in **B**. All of the coordinate bonds to the divalent nickel cation are in fact longer in **4**. Similarly, the bond C1−O1 in the carboxylate unit is longer, and as might be expected to accompany this, the C1−O2 bond is shorter. This is accompanied by a shortening of the mean carbon−carbon distance for the aromatic ring in **4**.

The helical framework alters to accommodate the bidentate *meso*-2,3-butanediol ligand. This is achieved by a series of small distortions to make the distance from the unfavorable methyl group to the framework (C12a‥B···O2) as long as possible. First, both metal−carboxylate and metal−diol coordinate bonds are longer for the *meso*-2,3-butanediol

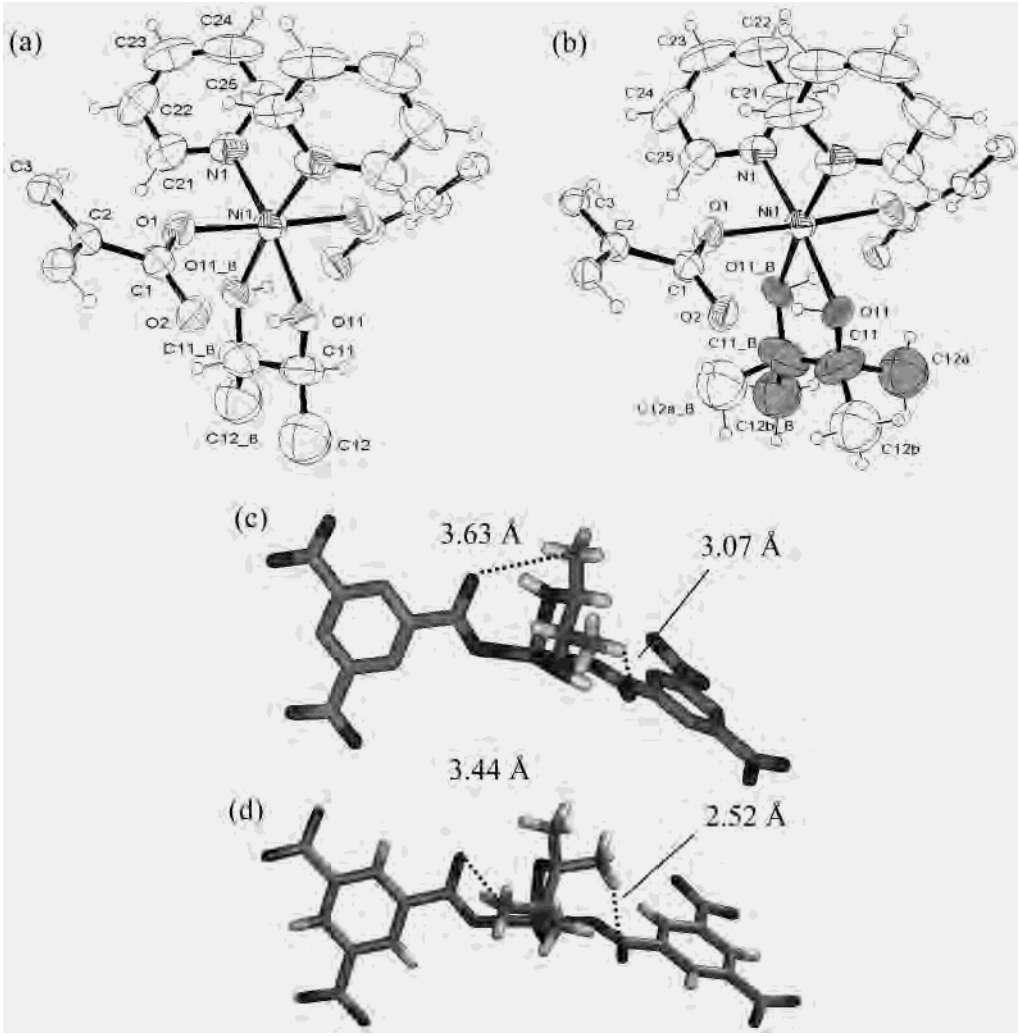

Figure 7. Nickel coordination for (a) 1,2-propanediol and (b) *meso*-2,3-butanediol **4** frameworks. One orientation of the *meso*-2,3-butanediol is colored gray. ORTEP plots are shown as 30% thermal ellipsoids. Atoms labeled_B are generated by the symmetry operator 1.25 − *y*, 1.25 − *x*, 0.25 − *z*. Diol geometries for bound (c) 1,2-propanediol and (d) *meso*-2,3-butanediol. Close contacts between the methyl groups and the framework are shown. For *meso*-2,3-butanediol, the diol displays both favored and disfavored chiral centers bound to the framework. Nonbonded contacts are shown for the disfavored center. For 1,2-propanediol, the distances shown are for the observed enantiomer.

ligand, which has the effect of pushing the methyl group away from the framework carbonyl. The carbonyl contracts a little which enhances this effect. While the O11_Ni_O11B bite angles of the two diols are similar, the most striking difference occurs in the geometry of the stereogenic centers in the pair of diols. The *meso*-2,3-butanediol shows some distortion so that the energetically disfavored methyl group (C12a) moves further away from the framework, while the other (C12b) moves slightly to accommodate this; the two secondary carbon atoms do not display perfect tetrahedral geometry (as indicated by the O11_C11_C12 angles in Table 2).

In these ways, the distance from C12a to O2 is lengthened, although for the 1,2-propanediol framework the methyl group of the diol (C12) is further from the Ni_3btc_2 framework in the observed isomer. The calculated distances for C12 and H12a to O2 for the disfavored (*R*) enantiomer bound to the 1,2-pd framework are 2.99(1) and 2.10(1) Å, while distortions about the metal described here increase these to 3.44(1) and 2.52(1) Å for the *meso*-2,3-butanediol ligand, allowing it to bind in bidentate fashion. The distortion occurs so that the geometry at the "favored" chiral center is no less favored than in the 1,2-propanediol case. The change in geometry of the diol ligand upon the change from 1,2-propanediol to *meso*-2,3-butanediol is illustrated in Figure 7c,d).

The templating effect of diols with the formulation RCH(OH)CH_2OH, such as 1,2-propanediol and (*S*,*S*)- and (*R*,*R*)-2,3-butanediol, has been demonstrated in four crystal structures.[33] The *R* enantiomer of 1,2-phenylethanediol directs, as predicted on the basis of the described examples of growth from racemic solvent, the growth of right-handed helices in the interpenetrating two-network structure in **5**. The origin of this templating is the disfavored binding of one diol enantiomer because it makes excessively close contacts with the framework of the opposite chirality. However, in the case of the achiral *meso*-2,3-butanediol, a molecule is bound which has the unfavorable configuration at one chiral center. There are distortions in the ligand and the framework local geometry to allow this. The unfavorable interaction which prevents the binding of *R*-1,2-propanediol to the left-handed network is significant enough to direct the growth of

Table 2. Selected Bond Distances and Angles for Frameworks Derived from 1,2-Propanediol and *meso*-2,3-Butanediol[a]

	inverted 1,2-propanediol	2,3-butanediol
Bond Lengths/Å		
Ni(1)−O(1)	2.008(4)	2.011(4)
Ni(1)−N(1)	2.078(6)	2.095(6)
Ni(1)−O(11)	2.086(5)	2.104(5)
O(1)−C(1)	1.250(7)	1.264(7)
O(2)−C(1)	1.260(7)	1.253(7)
C(1)−C(2)	1.486(5)	1.502(8)
mean ring C−C	1.400(8)	1.380(8)
O(11)−C(11)	1.40(1)	1.41(1)
C(11)−C(12)	1.49(3)	
C(11)−C(12a)		1.42(2)
C(11)−C(12b)		1.44(2)
C(11)−C(11)_B	1.60(3)	1.58(3)
Close Contacts		
C12a_B···O2	2.99(1)[b]	3.44(1)
H12a···O2	2.10(1)[b]	2.52(1)
Bond Angles/deg		
O(11)−Ni(1)−O(11)_B	82.3(3)	83.3(3)
O(11)−C(11)−C(12)	108(1)	
O(11)−C(11)−C(12a)		113(2)
O(11)−C(11)−C(12b)		105(2)
C(11)−O(11)−Ni(1)	111.4(6)	109.5(6)
O(11)−C(11)−C(11)_B	110.2(5)	111.7(7)
Torsion Angle		
C(3)_C−C(2)−C(1)−O(2)	12.1(1)	9.1(1)

[a] Shown in Figure 7. Symmetry operators used to generate equivalent atoms: B = 1.25 − *y*, 1.25 − *x*, 0.25 − *z*; C = $^1/_2$ + *z*, 1.5 − *x*, 1 − *y*. [b] Values for 1,2-pd contacts are calculated by inverting the chiral center of the observed, favored enantiomer to generate the disfavored enantiomer

homochiral networks. However, the demonstration of the growth of a framework from *meso*-2,3-butanediol which contains this interaction shows it to be a significant but small effect: the helix of the "incorrect" hand can grow with a given alcohol enantiomer, although significant distortions in the alcohol and network are required.

Triol Auxiliary Ligands. Both the triols studied, glycerol and 1,2,6-hexanetriol, contain the $RCH(OH)CH_2OH$ unit previously identified as directing the formation of two interpenetrating (10,3)-a networks. 1,2,6-Hexanetriol is found bound in bidentate fashion to the framework through the vicinal diol in **6**, with no evidence from the Fourier map for it being monodentate. The structure is entirely analogous to the parent phase **B**, and as expected, the handedness of the triol and network are in agreement. The alkyl chain of the triol is poorly resolved crystallographically, and a total of only five carbon atoms may be refined. The terminal carbon and one alcohol group of a 1,2,6-hexanetriol molecule may be refined in the extra-framework volume, where it is found forming one hydrogen bond (O···O 2.86(1) Å) to the carbonyl oxygen of a framework btc.

The glycerol structure **7** contains two interpenetrating Ni_3btc_2 (10,3)-a networks related by the body centering translation in the same way as the 1,2-propanediol phase. These networks have the same chirality, and the Flack parameter shows that single crystals are homochiral despite the binding of the achiral ligand glycerol. The most interesting feature is that the glycerol is observed both bidentate and monodentate to the divalent nickel cation. The coordination of the cation is shown in Figure 8 where the two different modes of coordination of the glycerol are highlighted.

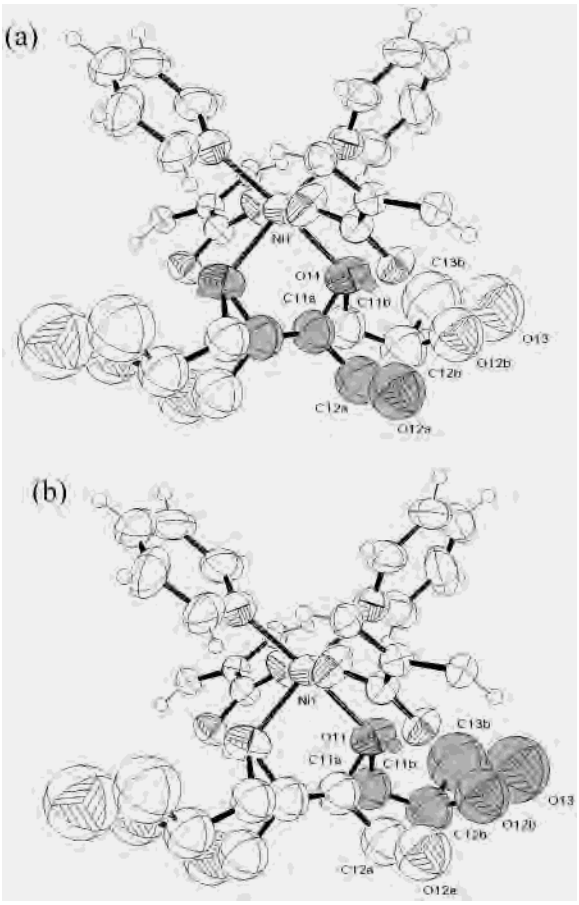

Figure 8. Coordination of Ni^{2+} in **7**. (a) Bidentate glycerol highlighted. (b) Monodentate glycerol highlighted.

As in previous examples, the ligand occupies two orientations about a two-fold axis which runs through the metal center (Wyckoff symmetry ..2). Refinement of the fraction of monodentate and bidentate glycerol with bond lengths restrained to chemically sensible distances shows that ratio is 45:55(1), resulting in the observed $Ni_3btc_2py_6(glycerol)_{4.3}$• guest composition. In each case, the cation coordination remains approximately octahedral. The presence of a significant proportion of monodentate glycerol can be explained because the monodentate binding allows the chain to form two hydrogen bonds. In the bidentate case, O12a forms a rather long hydrogen bond to one of the extra-framework molecules of glycerol (O···O is 3.08(3) Å). For the monodentate case, the relevant hydrogen bonds are from O13 to the free glycerol (O···O is 2.53(8) Å) and O12b (monodentate binding) to O12a (bidentate binding) where O···O is 2.89(5) Å. Metal centers 11.303(1) Å apart, in different networks, which are related by a two-fold rotation, participate in this hydrogen bonding. This will be maximized if one metal center has a single bidentate glycerol while the other has two monodentate glycerol molecules.

Discussion

The examples described here show how the structural features of this extensive family of interpenetrating network phases can be directed by simple chemical changes in the

auxiliary amine and alcohol ligands bound to the network-forming metal centers.

The introduction of 1,4-butanediol in place of ethylene glycol in the denser four network phase leads to a phase with different thermal behavior. The pores in the ethylene glycol system may be completely emptied by heating, but this is accompanied by ligand loss. Heating the 1,4-butanediol system to 140 °C drives out the extra-framework solvent without ligand loss and with only a very slight loss of crystallinity, to generate a highly crystalline material with vacant chiral pores, $Ni_3(btc)_2(py)_6(1,4\text{-bd})_4(\mu\text{-}1,4\text{-bd})$. This is a direct consequence of the structure: the bidentate diol acts not as a chelating ligand but as a bridge to link the helical networks covalently. As the dimensions of this ligand appear well-suited to network cross-linking in structures of this kind, it may be used in future together with other alcohols directly bound to the metal to produce cross-linked networks.

The replacement of pyridine in **A** with 4-picoline leads to **2** and **3** which are structurally very similar but crystallographically different. The introduction of an extra methyl group projecting into the extra-framework space leads to a significant reduction in the solvent available volume. The development of a homochiral phase with 1,2-propanediol bound to the framework opens up the possibility of chiral templating of the denser four network structure. Indeed, there is evidence that the 1,2-propanediol bound to the metal center is not racemic.

As 4-picoline allows the four network phase to be grown with the chiral 1,2-propanediol ligand bound in a monodentate manner to the metal, the chiral templating arising from this mode of binding can be compared with the bidentate model already established for the two network phase. In the two network phase **B**, recognition of the *S*-enantiomer by the left-handed network is complete: there is no crystallographic evidence for binding of the other enantiomer. This is in contrast to the four network phase **3** obtained from 4-picoline where the ratio of enantiomers bound is 60:40-(1). The reason for the reduced enantioselectivity is clear. The less hindered primary alcohol function of the 1,2-propanediol is bound to the metal, with the stereogenic secondary alcohol unit projecting into the extra-framework space and thus further from the helical network. The methyl group and hydroxyl are effectively fixed while the stereogenic carbon occupies one of two positions depending upon which enantiomer is bound. For the two enantiomers, the shortest atom to atom contacts are 3.63(1) and 3.18(1) Å to a 4-picoline auxiliary ligand in an adjacent network. The enantiomer with the longer contact is favored, but the shorter contact is obviously not very unfavorable as that enantiomer is also bound. For the two network phase, the close C···O contact of 2.99 Å to the network-forming btc prohibits the binding of the disfavored enantiomer. The difference in unfavorable contacts from 3.18 to 2.99 Å is small but significant, and it produces the observed strict recognition.

The term "templating" implies that the extended structure forms around a template because it is energetically favored. The use of the solid *R*-1,2 phenylethanediol in benzyl alcohol carrier solvent to grow the two-fold interpenetrated phase demonstrates that binding vicinal diols to the metal nodes of the 10,3-a network does specifically drive the formation of this network. The use of the resolved template also results in the predicted hand of the chiral helices matching that expected on the basis of growth from racemic solvents. The energetics involved in the recognition of the *S* diol by the left-handed helix must be very subtle, however, as it is possible to grow the two-fold interpenetrated 10,3-a net from *meso*-2,3-butanediol. Here, the diol is bidentate (the glycerol example shows it is possible to tolerate some monodentate diol in this structure, but the presence of bidentate diol thus far is a prerequisite for this phase to form), and this necessarily brings an unfavorable configuration close to the chiral helix which can only be of one defined hand. This unfavorable interaction is to some extent overcome by pronounced relaxation of the structure of both the network and the alcohol. This rearrangement is sufficient to allow the two-fold interpenetrated structure to grow. The formation of this structure is evidently sufficiently favorable to outweigh the small energetic differences between having one enantiomer or its opposite hand binding to a given network, as other competing M_3btc_2 structures such as the well-known layered phases[39] are not formed. The reduced chiral recognition in the case of the four network phase stabilized with monodentate 1,2-propanediol by 4-pyridine also reveals a key aspect of the chiral templating mechanism: the stereogenic center needs to be held close to the helix by binding to the metal for effective rejection of the incorrect enantiomer.

The simple assembly of readily available components into homochiral networks is possible using the metal/btc/alcohol/aromatic amine family, in which the networks are formed by the M and btc components, influenced by secondary structural effects from the auxiliary alcohol and amine ligands bound to the metal centers. The two basic interpenetrated (10,3)-a network structures are common to all the phases studied, but the structures can be controlled by simple and readily understandable variation in the auxiliary ligands bound to the framework-forming metal.

Acknowledgment. We thank the U.K. EPSRC for a studentship to T.J.P. and for support under GR/N08537. We thank Dr. S. Teat and Mr. J. F. Bickley for assistance with crystallographic data collection on the 9.8 (Daresbury SRS) and Stoë IPDS diffractometers, respectively.

Supporting Information Available: X-ray diffraction and thermal analysis data. ORTEP plot of the asymmetric unit of **2**. X-ray crystallographic file in CIF format. This material is available free of charge via the Internet at http://pubs.acs.org.

IC025775I

(39) Kepert, C. J.; Prior, T. J.; Rosseinsky, M. J. *J. Solid State Chem.* **2000**, *152*, 261−270.